

Direct Parameterization of Lipschitz-Bounded Deep Networks

Ruigang Wang, Ian R. Manchester*

Abstract

This paper introduces a new parameterization of deep neural networks (both fully-connected and convolutional) with guaranteed Lipschitz bounds, i.e. limited sensitivity to perturbations. The Lipschitz guarantees are equivalent to the tightest-known bounds based on certification via a semidefinite program (SDP), which does not scale to large models. In contrast to the SDP approach, we provide a “direct” parameterization, i.e. a smooth mapping from \mathbb{R}^N onto the set of weights of Lipschitz-bounded networks. This enables training via standard gradient methods, without any computationally intensive projections or barrier terms. The new parameterization can equivalently be thought of as either a new layer type (the *sandwich layer*), or a novel parameterization of standard feedforward networks with parameter sharing between neighbouring layers. We illustrate the method with some applications in image classification (MNIST and CIFAR-10).

1 Introduction

Neural networks have enjoyed wide application due to their many favourable properties, including highly accurate fits to training data, surprising generalisation performance within a distribution, and well as scalability to very large models and data sets. Nevertheless, it has also been observed that they can be highly sensitive to small input perturbations [1]. This is a critical limitation in applications in which certifiable robustness is required, or the smoothness of a learned function is important.

A standard way to quantify sensitivity of a models is via a *Lipschitz bound*, which generalises the notion of a slope-restricted scalar function. A learned function $x \mapsto f(x)$ between normed spaces satisfies a Lipschitz bound γ if

$$\|f(x_1) - f(x_2)\| \leq \gamma \|x_1 - x_2\|$$

for all x_1, x_2 in its domain. The (true) Lipschitz constant of a function is the smallest such γ .

A natural application of Lipschitz-bounds is to control a model’s sensitivity *adversarial* (worst-case) inputs, e.g. [2, 3], but Lipschitz constants also appear in bounds on statistical generalisation performance [4]. Lipschitz-bounds have been applied to help stabilise the learning of generative adversarial networks [5, 6], and more recently in implicit geometry mechanisms for computer graphics [7]. Lipschitz-bounded networks have also been investigated in the context of reinforcement learning and control problems, for controlling sensitivity to measurement noise (e.g. [8]) and ensuring robust stability of feedback loops during training [9]. In robotics applications, several learning-based planning and control algorithms require known Lipschitz bounds in learned stability certificates, see e.g. the recent surveys [10, 11].

Unfortunately, even for two-layer perceptions with ReLU activations, exact calculation of the true Lipschitz constant for ℓ^2 (Euclidean) norms is NP-hard [12], so attention has focused on approximations that balance accuracy with computational tractability. For l^1 and l^∞ norms, simple Lipschitz bounds can be expressed in terms of row and column sums of layer weights [13], but for l^2 it is more complex. Crude bounds can be found via the product of spectral norms of layer weights [1], however to date the most accurate bounds require solution of a semidefinite program (SDP) [14], which is computationally tractable only for relatively small fully-connected networks.

*R. Wang and I.R. Manchester are with Australian Centre for Field Robotics, The University of Sydney, Australia. E-mail: ruigang.wang, ian.manchester@sydney.edu.au

Furthermore, while *certification* of a Lipschitz bound of a fixed network is a (convex) SDP with this method, the set of weights satisfying a prescribed Lipschitz bound is highly non-convex, complicating training. Both [15] and [11] specifically highlight the computationally-intensive nature of these bounds as limitations for applications. We will continue to discuss related work below, but first we state the main contributions of this paper.

Contribution. In this paper we introduce a new parameterization of neural networks, both fully-connected multi-layer perceptions (MLP) and deep convolutional neural networks (CNN), which has *built-in* guarantees on the network’s Lipschitz bound, equivalent the best-known bounds provided by the SDP method [14]. Roughly speaking, we construct a smooth surjective mapping from an unconstrained parameter space \mathbb{R}^N onto the (non-convex) set of network weights satisfying these bounds.

This enables learning of lipschitz-bounded networks via standard unconstrained optimization methods such as stochastic gradient methods or ADAM [16], avoiding the complex projection steps or barrier function computations that have previously been required and limited scalability. In particular, to the authors knowledge this paper represents the first time that convolutional models for image classification have been successfully trained that satisfy the state-of-the-art Lipschitz bounds of [14].

Related Work. This work sits in the broader context of methods to certify safety and robustness of neural networks. This includes interval propagation bounds (see e.g. [17]) which are simple but can be conservative, to methods based on convex relaxation (e.g. [18] and [19]) and mixed-integer programming [20].

Specific to computation of Lipschitz bounds, [1] already suggested analysis via layer-wise spectral bounds. [3] proposed a computationally tractable approach for convolutional models, based one layer-wise estimates of spectral norm. [21] proposed a novel activation function and associated weight constraints. [13] presented training methods incorporating Lipschitz bounds for multiple norms, using a power iteration method to approximate spectral norms for the ℓ^2 case. [22] bounded Lipschitz constants via incremental dissipativity theory. Beyond standard feedforward networks, [23] proposed a class of Lipschitz-bounded equilibrium networks and [24] extended this to recurrent (dynamic) equilibrium networks.

Since the SDP-based bounds of [14] appeared, several papers have proposed methods to allow training of Lipschitz models. [25], which proposed an alternating direction method of multipliers (ADMM) approach, which required solving an SDP at each iteration. [26] and [27] improve computational tractability by exploiting chordal sparsity. Moving beyond the fully-connected case, [28] proposed a method based on 2D systems theory to certify 1D convolutional networks.

Notation. We let \mathbb{R}, \mathbb{C} be the set of real and complex numbers, respectively. The identity matrix is denoted by I . Throughout the paper we have

$$\begin{aligned} \mathbb{J}_+^n &:= \{\text{diagonal } J \in \mathbb{R}^{n \times n} \mid J_{ii} \in [0, 1], \forall 1 \leq i \leq n\}, \\ \mathbb{D}_{++}^n &:= \{\text{diagonal } D \in \mathbb{R}^{n \times n} \mid D_{ii} > 0, \forall 1 \leq i \leq n\}. \end{aligned}$$

$A \succeq 0$ means that A is positive semi-definite. For a vector $x \in \mathbb{R}^n$, its 2-norm is denoted by $\|x\|$. Given a matrix $A \in \mathbb{R}^{m \times n}$, $\|A\|$ is defined as its the largest singular value and A^+ is its generalized inverse.

2 Problem Setup and Preliminaries

Consider an L -layer feed-forward neural network $y = f(x)$ described by the following recursive equations:

$$\begin{aligned} z_0 &= x, \\ z_{k+1} &= \sigma(W_k z_k + b_k), \quad k = 0, \dots, L-1 \\ y &= W_L z_L + b_L, \end{aligned} \tag{1}$$

where $x \in \mathbb{R}^{n_0}$, $z_k \in \mathbb{R}^{n_k}$, $y \in \mathbb{R}^{n_{L+1}}$ are the network input, hidden unit of the k th layer and network output, respectively. Here $W_k \in \mathbb{R}^{n_{k+1} \times n_k}$ and $b_k \in \mathbb{R}^{n_{k+1}}$ are the weight matrix and bias vector for the k th layer. We make the following assumption on σ , which holds for commonly-used activation functions [29].

Assumption 2.1. The nonlinear activation $\sigma : \mathbb{R} \rightarrow \mathbb{R}$ is piecewise differentiable and sloped restricted in $[0, 1]$.

Note also that if different channels have different activation functions, then we simply require that they all satisfy the above assumption.

Definition 2.2. A feed-forward neural network f of the form (1) is said to be globally Lipschitz bounded by $\gamma > 0$ (or simply γ -Lipschitz) if

$$\|f(x_1) - f(x_2)\| \leq \gamma \|x_1 - x_2\|, \quad \forall x_1, x_2 \in \mathbb{R}^{n_0}. \quad (2)$$

Moreover, f is *nonexpansive* if it is 1-Lipschitz in ℓ^2 norm.

The main goal of this work is to learn feed-forward networks (1) with certificated Lipschitz bound of γ , i.e.,

$$\min_{\theta} \mathcal{L}(f_{\theta}) \quad \text{s.t.} \quad f_{\theta} \text{ is } \gamma\text{-Lipschitz} \quad (3)$$

where $\mathcal{L}(\cdot)$ is a loss function. Since it is NP-hard to compute the Lipschitz constant (i.e. the smallest Lipschitz bound) of f_{θ} . We need an accurate Lipschitz bound estimation so that the constraint in (3) does not lead to a significant restriction on the model expressivity.

In [14], integral quadratic constraint (IQC) theory was applied to capture both monotonicity and 1-Lipschitzness properties of σ , leading to a state-of-art tight Lipschitz bound estimation based on the following linear matrix inequality (LMI), see details in Appendix A:

$$H := \begin{bmatrix} \gamma I & -U^{\top} \Lambda & 0 \\ -\Lambda U & 2\Lambda - \Lambda W - W^{\top} \Lambda & -Y^{\top} \\ 0 & -Y & \gamma I \end{bmatrix} \succeq 0 \quad (4)$$

where $\Lambda \in \mathbb{D}_{++}^n$ with $n = \sum_{k=1}^L n_k$, and

$$W = \begin{bmatrix} 0 & & & \\ W_1 & \ddots & & \\ \vdots & \ddots & 0 & \\ 0 & \cdots & W_{L-1} & 0 \end{bmatrix}, \quad U = \begin{bmatrix} W_0 \\ 0 \\ \vdots \\ 0 \end{bmatrix},$$

$$Y = [0 \quad \cdots \quad 0 \quad W_L].$$

Although (4) can be converted into a convex constraint for Lipschitz bound estimation of a network with fixed W, U, Y , the learning problem in (3) is highly nonconvex due to changeable W, U, Y . For even relatively small-scale networks (e.g. ~ 1000 neurons), the associate barrier terms or projections become a major computational bottleneck.

Remark 2.3. The published paper [14] claimed that even tighter Lipschitz bounds could be achieved with a less restrictive class of multipliers Λ than diagonal. However, this claim was false: a counterexample was presented in [25], and an explanation of the error was presented in [23].

3 Model parameterization

In this section we will present a model parameterization (see Figure 1) such that the learning problem (3) with complicated matrix inequality constraint (4) can be transformed into an unconstrained optimization problem.

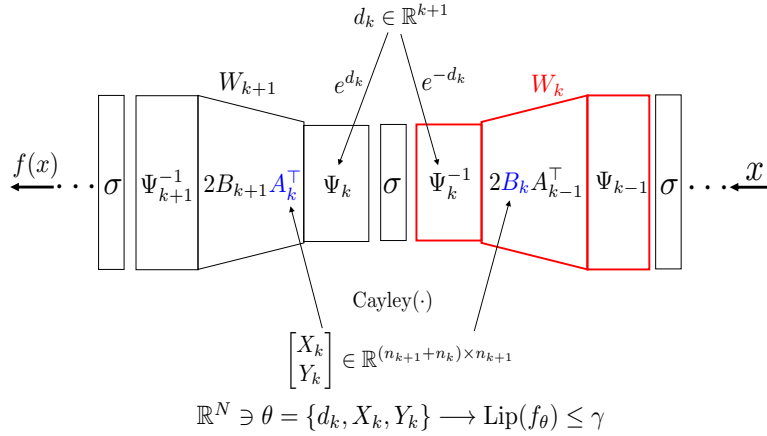


Figure 1: Direct parameterization for Lipschitz-bounded deep networks.

Definition 3.1. A mapping $\mathcal{M}_\Theta : \theta \in \Theta \subseteq \mathbb{R}^N \mapsto f_\theta$ is called a parameterization of DNNs with Lipschitz bound of γ if f_θ is γ -Lipschitz for any $\theta \in \Theta$. Furthermore, such mapping is called a *direct parameterization* if $\Theta = \mathbb{R}^N$.

The free parameter θ in the proposed direct parameterization consists of

$$d_j \in \mathbb{R}^{n_{j+1}}, \quad j = 0, \dots, L-1, \\ X_k \in \mathbb{R}^{n_{k+1} \times n_{k+1}}, Y_k \in \mathbb{R}^{n_k \times n_{k+1}}, \quad k = 0, \dots, L.$$

Note that bias terms are dropped for simplicity. Based these parameters, we first construct

$$\Psi_j = \text{diag}(e^{d_j}), \quad \begin{bmatrix} A_k \\ B_k \end{bmatrix}^\top = \text{Cayley} \left(\begin{bmatrix} X_k \\ Y_k \end{bmatrix} \right) \quad (5)$$

where the Cayley transform is defined as

$$\text{Cayley} \left(\begin{bmatrix} X \\ Y \end{bmatrix} \right) := \begin{bmatrix} (I+Z)^{-1}(I-Z) \\ -2Y(I+Z)^{-1} \end{bmatrix} \quad (6)$$

with $Z = X - X^\top + Y^\top Y$. Then, the weight matrices of (1) are given by

$$W_k = 2\Psi_k^{-1}B_kA_{k-1}^\top\Psi_{k-1}, \quad k = 0, \dots, L \quad (7)$$

where $A_{-1} = I, \Psi_{-1} = \sqrt{\gamma/2}I$ and $\Psi_L = \sqrt{2/\gamma}I$ with γ as the prescribed Lipschitz bound. Notice that weight k depends on parameters of index k and $k-1$, i.e. there is an ‘‘interlacing’’ coupling between parameters and weights.

The proposed approach is mainly based on the observation that the structure of H in (4) is a chordal graph. Thus, any semi-definite matrix with such structure can be parameterized by $H = PP^\top$ where

$$P = \begin{bmatrix} D_{-1} & & & & \\ -V_0 & D_0 & & & \\ & \ddots & \ddots & & \\ & & & -V_L & D_L \end{bmatrix}.$$

Substituting the above parameterization into (4) yields (6), see detailed derivation in Appendix B.

The main theoretical results is that our parameterization is *complete* (necessary and sufficient) for the set of DNNs satisfying the LMI constraint (4) of [14].

Theorem 3.2. *The forward network (1) satisfies the LMI condition (4) iff its weight matrices W_k can be parameterized via (7).*

The proof of this and all other theorems can be found in the appendix.

3.1 Nonexpansive sandwich layer

The proposed parameterization can also be interpreted as a new layer type. By introducing new hidden units $h_k = \sqrt{2}A_k^\top \Psi_k z_k$ for $k = 0, \dots, L$, we can rewrite the proposed γ -LBDN as

$$\begin{aligned} h_0 &= \sqrt{\gamma}x \\ h_{k+1} &= \sqrt{2}A_k^\top \Psi_k \sigma(\sqrt{2}\Psi_k^{-1}B_k h_k + b_k) \\ y &= \sqrt{\gamma}B_L h_L + b_L. \end{aligned} \tag{8}$$

The core component of the above model is a sandwich-structured layer of the form:

$$h_{\text{out}} = \sqrt{2}A^\top \Psi \sigma(\sqrt{2}\Psi^{-1}B h_{\text{in}} + b) \tag{9}$$

where $h_{\text{in}} \in \mathbb{R}^p, h_{\text{out}} \in \mathbb{R}^q$ are the layer input and output, respectively. Unlike the parameterization in (7), consecutive layers in (8) does not have coupled free parameters, which allows for modular implementation. Another advantage is that such representation can reveal some fundamental insights on the roles of Ψ, A and B .

Theorem 3.3. *The layer (9) with Ψ, A, B constructed by (5) is nonexpansive.*

To understand the role of Ψ , we look at a simple nonlinear activation layer which is obtained simply by placing $\Psi \in \mathbb{D}_{++}^q$ and its inverse after and before σ , i.e.,

$$u = \Psi \sigma(\Psi^{-1}v + b). \tag{10}$$

Here Ψ can change the shape and shift the position of individual activation channel while keeping their slopes within $[0, 1]$, allowing the optimizer to search over a rich set of activations.

For the roles of A and B , we need to look at another special case of (9) where σ is the identity operator. Then, (9) becomes a linear layer

$$h_{\text{out}} = 2A^\top B h_{\text{in}} + \hat{b}. \tag{11}$$

As a direct corollary of Theorem 3.3, the above linear layer is nonexpansive, i.e., $\|2A^\top B\| \leq 1$. We show that such parameterization is *complete* for nonexpansive linear layers.

Proposition 3.4. *A linear layer is nonexpansive iff its weight W satisfies $W = 2A^\top B$ with A, B given by (5).*

3.2 Nonexpansive convolutional layer

Our proposed layer parameterization can also incorporate more structured linear operators such as convolution. Let $h_{\text{in}} \in \mathbb{R}^{p \times s \times s}$ be a p -channel image tensor with $s \times s$ spatial domain and $h_{\text{out}} \in \mathbb{R}^{q \times s \times s}$ be q -channel output tensor. We also let $A \in \mathbb{R}^{q \times q \times s \times s}$ denote a multi-channel convolution operator and similarly for $B \in \mathbb{R}^{q \times p \times s \times s}$. For the sake of simplicity, we assume that the convolutional operators A, B are circular and unstrided. Such assumption can be easily related to plain and/or 2-strided convolutions, see [30]. Similar to (9), the proposed convolutional layer can be rewritten as

$$\text{Vec}(h_{\text{out}}) = \sqrt{2}\mathcal{C}_A^\top \Psi_s \sigma(\sqrt{2}\Psi_s^{-1}\mathcal{C}_B \text{Vec}(h_{\text{in}}) + b) \tag{12}$$

where $\mathcal{C}_A \in \mathbb{R}^{qs^2 \times qs^2}, \mathcal{C}_B \in \mathbb{R}^{qs^2 \times ps^2}$ are the doubly-circular matrix representations of A and B , respectively. For instance, $\text{Vec}(B * h_{\text{in}}) = \mathcal{C}_B \text{Vec}(h_{\text{in}})$ where $*$ is the convolution operator. We choose $\Psi_s = \Psi \otimes I_s$ with $\Psi = \text{diag}(e^d)$ so that individual channel has a constant scaling factor. To ensure that (12) is nonexpansive,

Algorithm 1 Nonexpansive convolutional layer

Require: $h_{\text{in}} \in \mathbb{R}^{p \times s \times s}$, $P \in \mathbb{R}^{(p+q) \times q \times s \times s}$, $d \in \mathbb{R}^q$

- 1: $\tilde{h}_{\text{in}} \leftarrow \text{FFT}(h_{\text{in}})$
 - 2: $\Psi \leftarrow \text{diag}(e^d)$, $[\tilde{A} \ \tilde{B}]^* \leftarrow \text{Cayley}(\text{FFT}(P))$
 - 3: $\tilde{h}[:, :, i, j] \leftarrow \sqrt{2}\Psi^{-1}\tilde{B}[:, :, i, j]\tilde{h}_{\text{in}}[:, :, i, j]$
 - 4: $\tilde{h} \leftarrow \text{FFT}(\sigma(\text{FFT}^{-1}(\tilde{h}) + b))$
 - 5: $\tilde{h}_{\text{out}}[:, :, i, j] \leftarrow \sqrt{2}A[:, :, i, j]^*\Psi\tilde{h}[:, :, i, j]$
 - 6: $h_{\text{out}} \leftarrow \text{FFT}^{-1}(\tilde{h}_{\text{out}})$
-

we need to construct $\mathcal{C}_A, \mathcal{C}_B$ using the Cayley transformation (6), which involves inverting a highly-structured large matrix $I + \mathcal{C}_Z \in \mathbb{R}^{qs^2 \times qs^2}$.

Thanks to the doubly-circular structure, we can perform efficient computation on the Fourier domain. Taking a 2D case for example, circular convolution of two matrices is simply the elementwise product of their representations in the Fourier domain [31]. In [30], the 2D convolution theorem was extended to multi-channel circular convolutions of tensors, which are reduced to a batch of complex matrix-vector products in the Fourier domain rather than elementwise products. For example, the Fourier-domain output related to the $(i, j)^{\text{th}}$ pixel is a matrix-vector product:

$$\text{FFT}(B * h_{\text{in}})[:, :, i, j] = \tilde{B}[:, :, i, j]\tilde{h}_{\text{in}}[:, :, i, j].$$

where $\tilde{B}[:, :, i, j] \in \mathbb{C}^{q \times p}$ and $\tilde{h}_{\text{in}}[:, :, i, j] \in \mathbb{C}^p$. Here $\tilde{x} = \text{FFT}(x)$ is the fast Fourier transformation (FFT) of a multi-channel tensor $x \in \mathbb{R}^{c_1 \times \dots \times c_r \times s \times s}$:

$$\text{FFT}(x)[i_1, \dots, i_r, :, :] = \mathcal{F}_s x[i_1, \dots, i_r, :, :] \mathcal{F}_s^*$$

where $\mathcal{F}_s[i, j] = \frac{1}{s} e^{-2\pi(i-1)(j-1)\iota/s}$ with $\iota = \sqrt{-1}$. Moreover, transposing or inverting a convolution is equivalent to applying the complex version of the same operation to its Fourier domain representation – a batch of small complex matrices:

$$\text{FFT}(A^\top)[:, :, i, j] = \tilde{A}[:, :, i, j]^*, \quad \text{FFT}((I + Z)^{-1})[:, :, i, j] = (I + \tilde{Z}[:, :, i, j])^{-1}.$$

Since the FFT of a real tensor is Hermitian-symmetric, the batch size can be reduced to $s \times (\lfloor s/2 \rfloor + 1)$.

We now give both model parameterization and forward computation of a nonexpansive convolutional layer in Algorithm 1. In line 1 and 6, we use the (inverse) FFT on the input/output tensor, which can be either/both removed for multiple consecutive convolutional layers. In line 2, we perform the Cayley transformation of convolutions in the Fourier domain, which involves $s \times (\lfloor s/2 \rfloor + 1)$ parallel complex matrix inverse of size $q \times q$. In line 3-5, all operations related to the $(i, j)^{\text{th}}$ term can be done in parallel.

3.3 Comparison to Semi-Orthogonal Layers

In this section we will compare the proposed approach to a closely related method developed in [30], which also applies the Cayley transform to construct non-expansive layers. We first compare from the layer point of view as both approaches provide parameterization for nonexpansive layers. We show that our layer parameterization is more general. Second, we compare the networks constructed from those two layers, in terms of layerwise spectral bound $\prod_{k=0}^L \|W_k\|$, which is a loose Lipschitz upper bound of the network Jacobian operator

$$\mathbf{J}^c f_\theta = W_L \prod_{k=1}^L J_{L-k} W_{L-k} \in \mathbb{R}^{n_{L+1} \times n_0}$$

where $J_k = \mathbf{J}^c \sigma(W_k z_k + b_k) \in \mathbb{J}_+^{n_{k+1}}$ with \mathbf{J}^c as the generalized Clarke Jacobian. It often leads to conservative results when training a 1-Lipschitz network subject to the naive bound $\prod_{k=0}^L \|W_k\| \leq 1$. We present some

theoretical analysis to show that our parameterization allows for both the individual layer and network spectral bound to be larger than 1, while the network Lipschitz constant is still bounded by a weighted layerwise spectral bound of 1. In the next section, we will illustrate this result using a toy example.

Layer-level comparison. The core component in [30] is the parameterization of (semi)-orthogonal layers via Cayley transformation. It takes a free variable $P \in \mathbb{R}^{q \times p}$ and then produce (semi)-orthogonal weight matrix via $W = \text{Cayley}(P)$.

However, for the case $p = q$, such parameterization is *incomplete* as it is limited to the orthogonal matrices without -1 eigenvalues. As shown in Proposition 3.4 our parameterization is complete, i.e., it includes any weight matrix whose eigenvalues within the unit disk, at the the cost of extra $q \times q$ parameters. Taking $p = q = 2$ for example, $\text{Cayley}(P)$ only contains rotation matrices while $2A^\top B$ can also include reflection matrices, e.g., we obtain $W = \text{diag}(-1, 1)$ via (6) with

$$X = \frac{1}{3} \begin{bmatrix} 0 & 0 \\ 2\sqrt{2} & 0 \end{bmatrix}, \quad Y = \frac{1}{3} \begin{bmatrix} 1 & \sqrt{2} \\ \sqrt{2} & -1 \end{bmatrix}.$$

Network-level comparison. The γ -LBDN constructed by semi-orthogonal layers has weight matrices of

$$W_k = \begin{cases} \sqrt{\gamma} \text{Cayley}(P_k), & k = 0, L \\ \text{Cayley}(P_k), & k = 1, \dots, L - 1, \end{cases} \quad (13)$$

where $P_k \in \mathbb{R}^{n_{k+1} \times n_k}$ is a free variable. It is easy to verify

$$\|W_0\| = \sqrt{\gamma}, \quad \|W_k\| = 1, \quad 0 \leq k < L, \quad \|W_L\| = \sqrt{\gamma},$$

which further provides the Lipschitz certification by $\|\mathbf{J}^c f\| \leq \prod_{k=0}^L \|W_k\| = \gamma$. However, such model set is quite restrictive as the bound estimation is quite loose. Our parameterization uses more sophisticated weighting (i.e. full matrices) for the spectral bounds, which leads to a more expressive model set.

Proposition 3.5. *The forward network with (7) satisfy the following weighted spectral bounds:*

$$\begin{cases} \|B_0^+ \Psi_0 W_0\| \leq \sqrt{2\gamma}, \\ \left\| \left\| B_k^\top \Psi_k W_k \Psi_{k-1}^{-1} (A_{k-1}^\top)^+ \right\| \right\| \leq 2, \quad 1 \leq k < L, \\ \|W_L \Psi_{L-1}^{-1} (A_{L-1}^\top)^+\| \leq \sqrt{2\gamma}, \end{cases}$$

which further implies that $\|\mathbf{J}^c f\| \leq \gamma$.

4 Experiments

Our experiments have two goals: First, to show that our model parameterization can provide a tight Lipschitz bounds, which we illustrate with simple curve-fitting tasks. Second, to examine the performance and scalability of the proposed new layer parameterization on adversarially robustness image classification tasks, illustrated with the MNIST and CIFAR-10 data sets. Throughout this section we use **sandwich** and **orthogon** to denote the LBDNs constructed from the proposed sandwich layer and orthogonal layer from [30], respectively. Further results and training details can be found in the appendix.

Tightness of Lipschitz Bounds. We illustrate the tight Lipschitz bound of our model parameterization some toy examples of curve fitting:

$$\begin{aligned} \text{square wave: } f(x) &= \begin{cases} 0, & x \in [-1, 0) \cup [1, 2] \\ 1, & x \in [-2, -1) \cup [0, 1) \end{cases} \\ \text{multi-sine: } f(x) &= \sin(x) + 0.2 \sin(5x), \quad x \in [0, 2\pi]. \end{aligned} \quad (14)$$

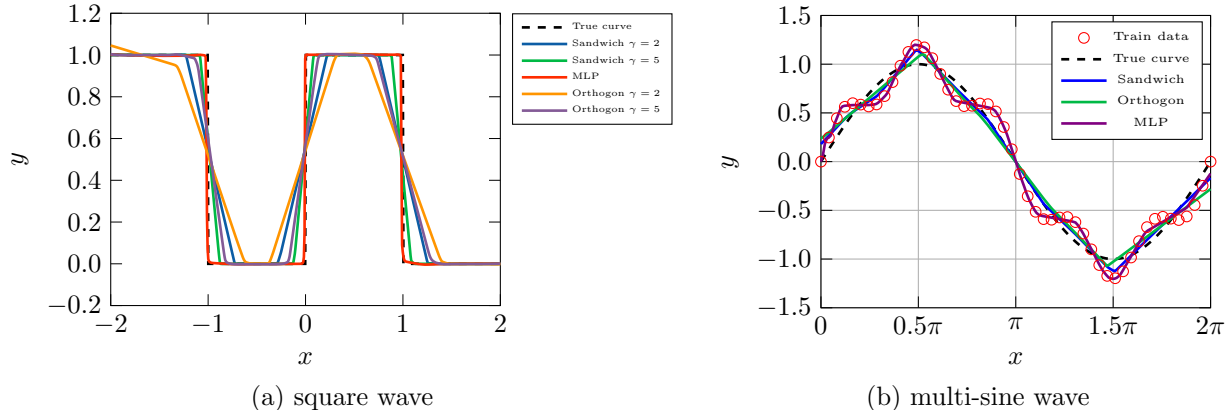


Figure 2: Simple 1D curve-fitting tasks with Lipschitz bound constraints.

The results are illustrated in Fig. 2. Table 1 includes details of the model structures and numerical results of the fitting. Note that we used wider layers for the orthogonal and MLP layers in order to approximately match the total number of parameters with the sandwich layer.

For the square wave, the true function has no global Lipschitz bound due to the points of discontinuity. Thus a function approximator will naturally try to find models with large local Lipschitz constant near those singular points, and if a global γ -Lipschitz constraint is imposed this is a useful test of its accuracy. We evaluate the tightness of Lipschitz bound using $\underline{\gamma}/\gamma$ where $\underline{\gamma}$ is an empirical lower Lipschitz bound obtained by a PGD-like method and γ is the imposed upper bound, which was 1, 2, and 5 in the cases we tested. In Table 1 it can be seen that our approach achieves a much tighter Lipschitz bounds for all three cases, roughly 99% versus 75% for orthogonal layer.

In Figure 3 we break down the Lipschitz bounds and spectral norms over layers. It can be seen that both the orthogonal layer $z_k \rightarrow z_{k+1}$ and sandwich layer $h_k \rightarrow h_{k+1}$ have quite tight Lipschitz bounds on a per-layer basis of around 98%. However, for the complete network the sandwich layer achieves a much tighter bound of 99.6% vs 75%. This illustrates the benefits of taking into account coupling between neighborhood layers, thus allowing individual layers to have spectral norm greater than 1. We note that, for the sandwich model, the layer-wise product of spectral norms reaches 122.2, illustrating how poor this commonly-used bound is compared to our bound.

For the multi-sine, we have a sum of a low-frequency sine wave and high-frequency sine-waves, each of which individually have a maximum slope (Lipschitz bound) of 1, and the true Lipschitz constant is 2 (achieved at $x = \pi$). We fit Lipschitz-bounded MLP models using the proposed sandwich layers and orthogonal layers. It can be seen in Table 1 that the tightness of our Lipschitz bound is 98.4%, whereas for the orthogonal layers it is only 61.3%. The MLP model has a maximum slope of 4.051, despite the actual curve being fit having a maximum slope of 2.

Adversarial Robust Training of Image Classifiers. We next examine an application in image classification, using the Lipschitz bounds to enhance adversarial robustness.

The first case we considered was the MNIST data set with fully-connected layers. In Figure 4 we observe that the sandwich layer had lower test error than the orthogonal layer in all cases, illustrating the improved flexibility. Both layers achieved have similarly tight Lipschitz bounds, however the were not nearly as tight as in the curve fitting case. We note that with $\gamma = 0.1$ both models offer significant robustness advantages to adversarial perturbations, while Sandwich offers better nominal test error than MLP, but Orthogonal degrades test error. In fact, the sandwich layer with $\gamma = 0.1$ achieves similar test error to the orthogonal layer $\gamma = 0.5$ and 1, while offering much better robustness.

For CIFAR10 we fit multi-layer convolutional models, and see similar trends. We note that this is, to our knowledge, the first experimental result of multi-layer 2D convolutional models satisfying the Lipschitz bounds

Table 1: Hyperparameters and Lipschitz bounds for the 1D curve fitting tasks.

	Square wave			Sine wave		
	SANDWICH	ORTHOGON	MLP	SANDWICH	ORTHOGON	MLP
FC: DEPTH×WIDTH	8×90	8×128	8×128	8×90	8×128	8×128
NUM. PARAMS	139,512	132,491	132,481	139,512	132,491	132,481
MAX. LR	0.01	0.01	0.01	0.005	0.05	0.01
EPOCHS	200	200	200	400	400	400
EMP. $\underline{\gamma}$ / CERT. γ	0.998 /1.0	0.738/1.0	106.7/-	0.984 /1.0	0.613/1.0	4.051/-
EMP. $\underline{\gamma}$ / CERT. γ	1.998 /2.0	1.472/2.0	-	-	-	-
EMP. $\underline{\gamma}$ / CERT. γ	4.950 /5.0	3.355/5.0	-	-	-	-

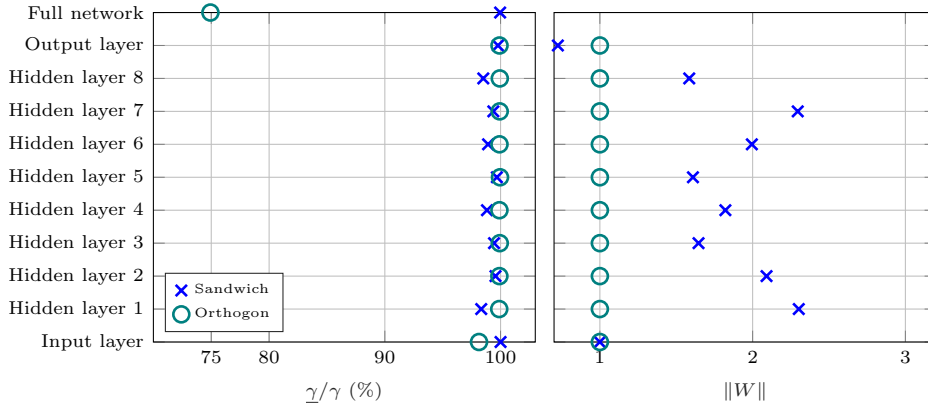


Figure 3: **Left:** empirical Lipschitz bound for curve fitting of a square wave. The lower bound $\underline{\gamma}$ is obtained using PGD-like method. We observed tight layer Lipschitz bound for both orthogonal and sandwich layers ($\geq 98.1\%$). However, the propose sandwich layer has a much tighter Lipschitz bound for the entire network (99.6% versus 75%). **Right:** the spectral norm of weight matrices. Our approach admits weight matrices with spectral norm larger than 1. The layerwise product $\prod_{k=0}^L \|W_k\|$ is about 122.2, which is much larger than that of orthogonal layers.

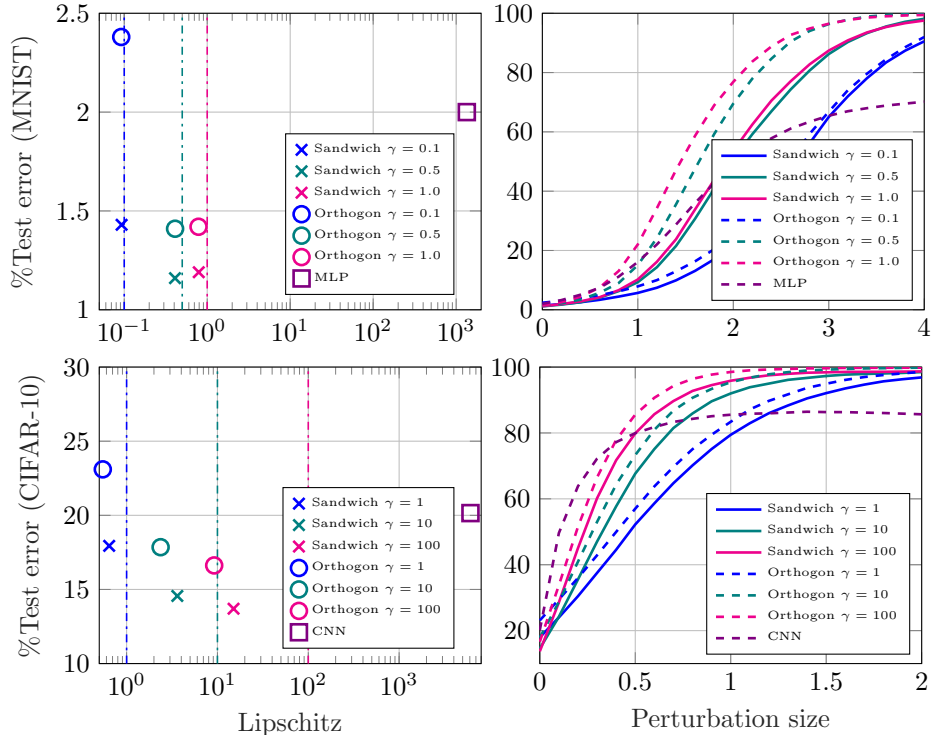


Figure 4: Image classification: test error vs Lipschitz constants (left) and robustness to adversarial perturbations (right), for MNIST with fully-connected layers (top) and CIFAR-10 with convolutional layers (bottom). Note that the proposed sandwich layer achieves both better test error and greater robustness than alternatives.

of [14]. Again we see that Lipschitz bounds improve test error compared to a vanilla CNN, while also improving robustness dramatically. And again, the sandwich layer with $\gamma = 1$ achieves similar test error to the orthogonal layer with $\gamma = 10$, while offering much better robustness, see additional results in Table 2.

A major aim of our paper is to make the Lipschitz bounds of [14] tractable for training of larger models, compared to previous methods that depended on semidefinite programming. In Figure 5 we plot the training curves (test-error vs epoch) and the computational time per epoch for the sandwich, orthogonal, and MLP/CNN models for MNIST (fully-connected models) and CIFAR-10 (convolutional models). Firstly, we observe that for both fully-connected and convolutional models, the training time per epoch of the sandwich model is only around double that of a vanilla model. Furthermore, this is offset by the fact that in both cases the sandwich model surpasses the final error of the MLP/CNN in less than half as many epochs. In fact, for the fully connected case it does so in around a third as many epochs.

An interesting observation from Figure 5 is that both the MLP and CNN models seem to exhibit the epoch-wide double descent phenomenon (see, e.g., [32]), whereas neither of the Lipschitz bounded models (sandwich and orthogonal) do, they simply improve test error monotonically with epochs. Weight regularization has been suggested as a mitigating factor for other forms of double descent [33], however we are not aware of this specific phenomenon having been observed before.

5 Conclusions and Future Work

In this paper we have introduced a new parameterization of neural networks that automatically satisfy the tightest currently-known computationally-tractable Lipschitz bounds. This enables learning of Lipschitz-

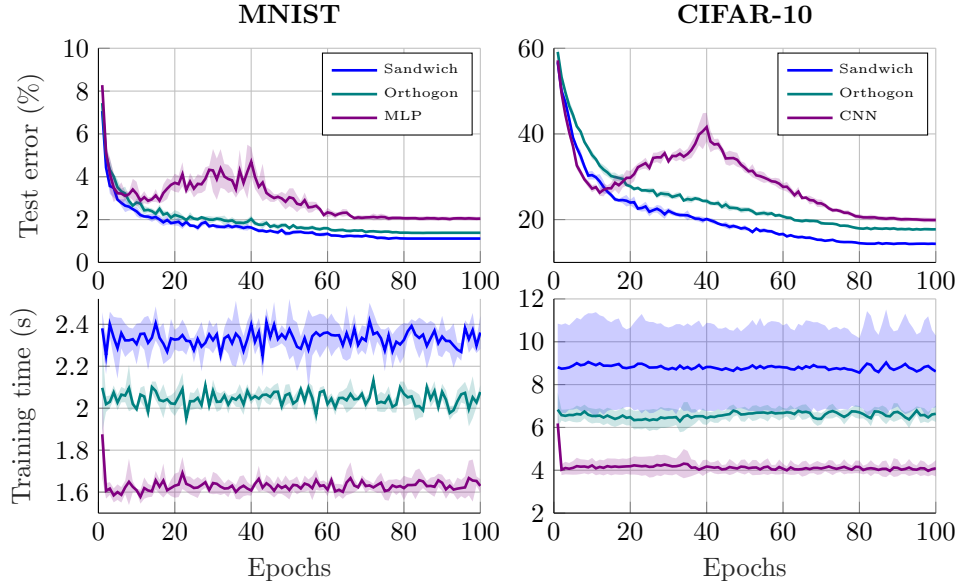


Figure 5: Learning curves and training time per epoch for image classification tasks, obtained from 5 experiments. The Lipschitz bounds are 0.5 for MNIST and 10 for CIFAR-10. Note that the “double-descent” phenomenon is avoided with the Lipschitz-bounded models.

Table 2: Test error, empirical adversarial robustness and empirical lower Lipschitz bound on image classification benchmarks, mean and standard deviation from 5 experiments. Sandwich layers outputs other methods in both test and ℓ_2 certifiable robust accuracy.

		MNIST						
		SANDWICH			ORTHOOGON			MLP
CERT. γ		0.1	0.5	1.0	0.1	0.5	1.0	–
EMP. $\underline{\gamma}$		9.32±.06E-2	0.41±.01	0.78±.01	9.15±.07E-2	0.41±.01	0.78±.01	1.0±.3E3
ERR. $\epsilon = 0.0$		1.37±.05	1.11±.05	1.19±.05	2.42±.04	1.38±.03	1.42±.05	2.05±.10
ERR. $\epsilon = 0.2$		1.85±.05	1.75±.05	1.87±.07	3.12±.08	2.21±.05	2.49±.10	3.47±.24
		CIFAR						
		SANDWICH			ORTHOOGON			CNN
CERT. γ		1	10	100	1	10	100	–
EMP. $\underline{\gamma}$		0.64±.00	3.51±.07	14.80±.67	0.53±.01	2.48±.07	9.45±.26	0.56±.12E4
ERR. $\epsilon = 0.0$		18.24±.25	14.34±.26	13.39±.52	22.96±.26	17.73±.33	17.07±.45	19.89±.59
ERR. $\epsilon = 0.1$		24.08±.28	23.72±.39	28.05±.70	29.34±.16	28.90±.11	34.71±.62	49.85±1.07

bounded networks with standard first-order gradient methods, avoiding the need for complex projections or barrier evaluations. We have illustrated the approach on simple curve-fitting tasks and adversarially-robust image classification with both fully-connected and convolutional networks.

Our future work will include exploring applications in other settings including robust reinforcement learning and control. We also note that the current approach to convolutional models (Sec 3.2) is limited to doubly-circular convolutions, which we will seek to address in the future.

References

- [1] C. Szegedy, W. Zaremba, I. Sutskever, J. Bruna, D. Erhan, I. Goodfellow, and R. Fergus, “Intriguing properties of neural networks,” in *ICLR: International Conference on Learning Representations*, 2014.
- [2] A. Madry, A. Makelov, L. Schmidt, D. Tsipras, and A. Vladu, “Towards deep learning models resistant to adversarial attacks,” in *International Conference on Learning Representations*, 2018.
- [3] Y. Tsuzuku, I. Sato, and M. Sugiyama, “Lipschitz-margin training: Scalable certification of perturbation invariance for deep neural networks,” in *Advances in neural information processing systems*, pp. 6541–6550, 2018.
- [4] P. L. Bartlett, D. J. Foster, and M. J. Telgarsky, “Spectrally-normalized margin bounds for neural networks,” in *Advances in Neural Information Processing Systems*, pp. 6240–6249, 2017.
- [5] M. Arjovsky, S. Chintala, and L. Bottou, “Wasserstein generative adversarial networks,” in *International conference on machine learning*, pp. 214–223, PMLR, 2017.
- [6] I. Gulrajani, F. Ahmed, M. Arjovsky, V. Dumoulin, and A. C. Courville, “Improved training of wasserstein gans,” *Advances in neural information processing systems*, vol. 30, 2017.
- [7] H.-T. D. Liu, F. Williams, A. Jacobson, S. Fidler, and O. Litany, “Learning smooth neural functions via lipschitz regularization,” in *ACM SIGGRAPH 2022 Conference Proceedings*, pp. 1–13, 2022.
- [8] A. Russo and A. Proutiere, “Towards optimal attacks on reinforcement learning policies,” in *2021 American Control Conference (ACC)*, pp. 4561–4567, IEEE, 2021.
- [9] R. Wang and I. R. Manchester, “Youla-ren: Learning nonlinear feedback policies with robust stability guarantees,” in *2022 American Control Conference (ACC)*, pp. 2116–2123, 2022.
- [10] L. Brunke, M. Greeff, A. W. Hall, Z. Yuan, S. Zhou, J. Panerati, and A. P. Schoellig, “Safe learning in robotics: From learning-based control to safe reinforcement learning,” *Annual Review of Control, Robotics, and Autonomous Systems*, vol. 5, pp. 411–444, 2022.
- [11] C. Dawson, S. Gao, and C. Fan, “Safe control with learned certificates: A survey of neural lyapunov, barrier, and contraction methods for robotics and control,” *IEEE Transactions on Robotics*, 2023.
- [12] A. Virmaux and K. Scaman, “Lipschitz regularity of deep neural networks: analysis and efficient estimation,” *Advances in Neural Information Processing Systems*, vol. 31, 2018.
- [13] H. Gouk, E. Frank, B. Pfahringer, and M. J. Cree, “Regularisation of neural networks by enforcing lipschitz continuity,” *Machine Learning*, vol. 110, pp. 393–416, 2021.
- [14] M. Fazlyab, A. Robey, H. Hassani, M. Morari, and G. Pappas, “Efficient and accurate estimation of lipschitz constants for deep neural networks,” in *Advances in Neural Information Processing Systems*, pp. 11427–11438, 2019.
- [15] M. Rosca, T. Weber, A. Gretton, and S. Mohamed, “A case for new neural networks smoothness constraints,” in *“I Can’t Believe It’s Not Better!” NeurIPS 2020 workshop*.
- [16] D. P. Kingma and J. L. Ba, “Adam: A method for stochastic gradient descent,” in *ICLR: International Conference on Learning Representations*, 2015.
- [17] S. Gowal, K. Dvijotham, R. Stanforth, R. Bunel, C. Qin, J. Uesato, R. Arandjelovic, T. Mann, and P. Kohli, “On the effectiveness of interval bound propagation for training verifiably robust models,” *arXiv preprint arXiv:1810.12715*, 2018.

- [18] A. Raghunathan, J. Steinhardt, and P. Liang, “Certified Defenses against Adversarial Examples,” in *International Conference on Learning Representations*, 2018.
- [19] E. Wong and Z. Kolter, “Provable defenses against adversarial examples via the convex outer adversarial polytope,” in *International conference on machine learning*, pp. 5286–5295, PMLR, 2018.
- [20] V. Tjeng, K. Y. Xiao, and R. Tedrake, “Evaluating robustness of neural networks with mixed integer programming,” in *International Conference on Learning Representations*, 2019.
- [21] C. Anil, J. Lucas, and R. Grosse, “Sorting out lipschitz function approximation,” in *International Conference on Machine Learning*, pp. 291–301, PMLR, 2019.
- [22] B. Aquino, A. Rahnama, P. Seiler, L. Lin, and V. Gupta, “Robustness against adversarial attacks in neural networks using incremental dissipativity,” *IEEE Control Systems Letters*, vol. 6, pp. 2341–2346, 2022.
- [23] M. Revay, R. Wang, and I. R. Manchester, “Lipschitz bounded equilibrium networks,” *arXiv:2010.01732*, 2020.
- [24] M. Revay, R. Wang, and I. R. Manchester, “Recurrent equilibrium networks: Unconstrained learning of stable and robust dynamical models,” in *2021 60th IEEE Conference on Decision and Control (CDC)*, pp. 2282–2287, IEEE, 2021.
- [25] P. Pauli, A. Koch, J. Berberich, P. Kohler, and F. Allgöwer, “Training robust neural networks using lipschitz bounds,” *IEEE Control Systems Letters*, vol. 6, pp. 121–126, 2021.
- [26] M. Newton and A. Papachristodoulou, “Exploiting sparsity for neural network verification,” in *Learning for Dynamics and Control*, pp. 715–727, PMLR, 2021.
- [27] A. Xue, L. Lindemann, A. Robey, H. Hassani, G. J. Pappas, and R. Alur, “Chordal sparsity for lipschitz constant estimation of deep neural networks,” in *2022 IEEE 61st Conference on Decision and Control (CDC)*, pp. 3389–3396, IEEE, 2022.
- [28] P. Pauli, D. Gramlich, and F. Allgöwer, “Lipschitz constant estimation for 1d convolutional neural networks,” *arXiv preprint arXiv:2211.15253*, 2022.
- [29] I. Goodfellow, Y. Bengio, and A. Courville, *Deep learning*. MIT press, 2016.
- [30] A. Trockman and J. Z. Kolter, “Orthogonalizing convolutional layers with the cayley transform,” *arXiv preprint arXiv:2104.07167*, 2021.
- [31] A. K. Jain, *Fundamentals of digital image processing*. Prentice-Hall, Inc., 1989.
- [32] P. Nakkiran, G. Kaplun, Y. Bansal, T. Yang, B. Barak, and I. Sutskever, “Deep double descent: Where bigger models and more data hurt,” *Journal of Statistical Mechanics: Theory and Experiment*, vol. 2021, no. 12, p. 124003, 2021.
- [33] P. Nakkiran, P. Venkat, S. M. Kakade, and T. Ma, “Optimal regularization can mitigate double descent,” in *International Conference on Learning Representations*, 2021.
- [34] Y.-C. Chu and K. Glover, “Bounds of the induced norm and model reduction errors for systems with repeated scalar nonlinearities,” *IEEE Transactions on Automatic Control*, vol. 44, no. 3, pp. 471–483, 1999.
- [35] F. J. D’Amato, M. A. Rotea, A. Megretski, and U. Jönsson, “New results for analysis of systems with repeated nonlinearities,” *Automatica*, vol. 37, no. 5, pp. 739–747, 2001.
- [36] V. V. Kulkarni and M. G. Safonov, “All multipliers for repeated monotone nonlinearities,” *IEEE Transactions on Automatic Control*, vol. 47, no. 7, pp. 1209–1212, 2002.

- [37] Y. Zheng, G. Fantuzzi, and A. Papachristodoulou, “Chordal and factor-width decompositions for scalable semidefinite and polynomial optimization,” *Annual Reviews in Control*, vol. 52, pp. 243–279, 2021.
- [38] Q. Li, S. Haque, C. Anil, J. Lucas, R. B. Grosse, and J.-H. Jacobsen, “Preventing gradient attenuation in lipschitz constrained convolutional networks,” *Advances in neural information processing systems*, vol. 32, 2019.
- [39] C. Coleman, D. Narayanan, D. Kang, T. Zhao, J. Zhang, L. Nardi, P. Bailis, K. Olukotun, C. Ré, and M. Zaharia, “Dawnbench: An end-to-end deep learning benchmark and competition,” *Training*, vol. 100, no. 101, p. 102, 2017.
- [40] D. P. Kingma and J. Ba, “Adam: A method for stochastic optimization,” *arXiv preprint arXiv:1412.6980*, 2014.
- [41] E. Winston and J. Z. Kolter, “Monotone operator equilibrium networks,” *Advances in neural information processing systems*, vol. 33, pp. 10718–10728, 2020.
- [42] J. Rauber, W. Brendel, and M. Bethge, “Foolbox: A python toolbox to benchmark the robustness of machine learning models,” *arXiv preprint arXiv:1707.04131*, 2017.

A Preliminaries on LMI-based Lipschitz bound estimation

Here we review the theoretical work of LMI-based Lipschitz bound estimation for neural networks from [14, 23]. Consider an L -layer forward network $y = f(x)$ described by the following recursive equation:

$$\begin{aligned} z_0 &= x, \\ z_{k+1} &= \sigma(W_k z_k + b_k), \quad k = 0, \dots, L-1, \\ y &= W_L z_L + b_L, \end{aligned} \tag{15}$$

where $x \in \mathbb{R}^{n_0}$, $z_k \in \mathbb{R}^{n_k}$, $y \in \mathbb{R}^{n_{L+1}}$ are the network input, hidden unit of the k th layer and network output, respectively. We stack all hidden unit z_1, \dots, z_L together and obtain a compact form of (15) as follows:

$$\begin{aligned} \underbrace{\begin{bmatrix} z_1 \\ z_2 \\ \vdots \\ z_L \end{bmatrix}}_z &= \sigma \left(\underbrace{\begin{bmatrix} 0 & & & \\ W_1 & \ddots & & \\ \vdots & \ddots & 0 & \\ 0 & \dots & W_{L-1} & 0 \end{bmatrix}}_W \underbrace{\begin{bmatrix} z_1 \\ z_2 \\ \vdots \\ z_L \end{bmatrix}}_z + \underbrace{\begin{bmatrix} W_0 \\ 0 \\ \vdots \\ 0 \end{bmatrix}}_U x + \underbrace{\begin{bmatrix} b_0 \\ b_1 \\ \vdots \\ b_{L-1} \end{bmatrix}}_{b_z} \right), \\ y &= \underbrace{\begin{bmatrix} 0 & \dots & 0 & W_L \end{bmatrix}}_Y \underbrace{\begin{bmatrix} z_1 \\ z_2 \\ \vdots \\ z_L \end{bmatrix}}_z + \underbrace{\begin{bmatrix} b_y \\ b_L \end{bmatrix}}_{b_y}. \end{aligned} \tag{16}$$

By introducing an intermediate variable $v \in \mathbb{R}^n$ with $n = \sum_{k=1}^L n_k$, we can rewrite the above equation by

$$v = Wz + Ux + b_z, \quad z = \sigma(v), \quad y = Yz + b_y. \tag{17}$$

Given two different solutions $s^a = (x^a, v^a, z^a, y^a)$ and $s^b = (x^b, v^b, z^b, y^b)$, their difference $\Delta s = s^b - s^a$ satisfies

$$\Delta v = W\Delta z + U\Delta x, \quad \Delta z = \sigma(v^b) - \sigma(v^a) := J^{ab}\Delta v, \quad \Delta y = Y\Delta z \tag{18}$$

where $J^{ab} \in \mathbb{J}_+^q$. For any Lipschitz bound $\gamma > 0$ we have $\gamma^2 \|\Delta x\|^2 - \|\Delta y\|^2 \geq 0$ holds for all nonzero Δs satisfying (18). The main challenge is how to handle the varying weight J^{ab} . One way is to replace it with a quadratic inequality constraint, which might be conserve but easy to analyze.

By substituting it back into (22) we have

$$D_{-1}D_{-1}^\top = \gamma I, \quad V_k V_k^\top + D_k D_k^\top = 2\Lambda_k, \quad 0 \leq k < L, \quad V_L V_L^\top + D_L D_L^\top = \gamma I, \quad (23)$$

$$W_k = \Lambda_k^{-1} V_k D_{k-1}^\top. \quad (24)$$

By defining $\Psi_k = \Lambda_k^{\frac{1}{2}}$, $A_k := \sqrt{2}\Psi_k D_k$ and $B_k := \sqrt{2}\Psi_k V_k^\top$ with $k = 0, \dots, L-1$ we have $A_k A_k^\top + B_k B_k^\top = I$. Then, we can easily parameterize (Ψ_k, A_k, B_k) via simple exponential mapping of diagonal matrices and Cayley transformation on full matrices, see (6). Finally, we can obtain the weight matrices as follows

$$W_k = \Lambda_k^{-1} V_k D_{k-1}^\top = \Psi_k^{-2} \times (\sqrt{2}\Psi_k B_k) \times (\sqrt{2}A_{k-1}^\top \Psi_{k-1}) = 2\Psi_k^{-1} B_k A_{k-1}^\top \Psi_{k-1} \quad (25)$$

with $k = 0, \dots, L-1$, where $A_{-1} = I$ and $\Psi_{-1} = \sqrt{\gamma/2}I$. The above formula can also be applied to $k = L$ by choosing $\Psi_L = \sqrt{2/\gamma}I$.

C Proofs

C.1 Proof of Lemma A.1

By substituting $\Delta z = J^{ab}\Delta v$ into (19) we have

$$\begin{bmatrix} \Delta v^\top \\ \Delta z^\top \end{bmatrix}^\top \begin{bmatrix} 0 & \Lambda \\ \Lambda & -2\Lambda \end{bmatrix} \begin{bmatrix} \Delta v \\ \Delta z \end{bmatrix} = 2\Delta z^\top \Lambda (\Delta v - \Delta z) = 2\Delta v^\top J^{ab} \Lambda (I - J^{ab}) \Delta v \geq 0$$

where the last inequality follows as $J^{ab} \in \mathbb{J}_+^q$.

C.2 Proof of Theorem A.3

We first apply Schur complement to (20), which yields

$$\begin{bmatrix} \gamma I & -U^\top \Lambda \\ -\Lambda U & 2\Lambda - \Lambda W - W^\top \Lambda - \frac{1}{\gamma} Y^\top Y \end{bmatrix} \succ 0.$$

Then, by left-multiplying the above equation by $[\Delta x^\top \quad \Delta z^\top]$ and right-multiplying $[\Delta x^\top \quad \Delta z^\top]^\top$ we can obtain

$$\gamma \|\Delta x\|^2 - \frac{1}{\gamma} \|\Delta y\|^2 - 2\Delta z^\top \Lambda \Delta z - 2\Delta z^\top \Lambda (W \Delta z + U \Delta x) = \gamma \|\Delta x\|^2 - \frac{1}{\gamma} \|\Delta y\|^2 - 2\Delta z^\top \Lambda (\Delta z - \Delta v) \geq 0, \quad (26)$$

which further implies that (15) is γ -Lipschitz since

$$\gamma \|\Delta x\|^2 - \frac{1}{\gamma} \|\Delta y\|^2 \geq 2\Delta z^\top \Lambda (\Delta v - \Delta z) \geq 0$$

where the last inequality follows by Lemma A.1.

C.3 Proof of Theorem 3.2

Sufficient. We show that (20) holds with $\Lambda = \text{diag}(\Lambda_0, \dots, \Lambda_{L-1})$ where $\Lambda_k = \Psi_k^2$. Since the structure of H is a chordal graph, $H \succeq 0$ is equivalent to the existence of a chordal decomposition [37]:

$$H = \sum_{k=0}^L E_k H_k E_k^\top \quad (27)$$

where $0 \preceq H_k \in \mathbb{R}^{(n_k+n_{k+1}) \times (n_k+n_{k+1})}$ and $E_k = [\mathbf{0}_{a,k} \quad \mathbf{I}_{b,k} \quad \mathbf{0}_{c,k}]$ with $\mathbf{I}_{b,k}$ being the identity matrix the same size as H_k , and $\mathbf{0}_{a,k}, \mathbf{0}_{c,k}$ being zero matrices of appropriate dimension. We then construct H_k as follows.

For $k = 0$, we take

$$H_0 = \begin{bmatrix} \gamma I & -\sqrt{2\gamma} B_0^\top \Psi_0 \\ -\sqrt{2\gamma} \Psi_0 B_0 & 2\Psi_0(I - A_0 A_0^\top) \Psi_0 \end{bmatrix}. \quad (28)$$

Note that $H_0 \succeq 0$ since $[H_0]_{11} = \gamma I \succ 0$, and the Schur complement to $[H_0]_{11}$ yields

$$2\Psi_0(I - A_0 A_0^\top) \Psi_0 - \sqrt{2\gamma} \Psi_0 B_0 \frac{1}{\gamma} I \sqrt{2\gamma} B_0^\top \Psi_0 = 2\Psi_0(I - A_0 A_0^\top - B_0 B_0^\top) \Psi_0 = 0.$$

For $k = 1, \dots, L-1$ we take

$$H_k = \begin{bmatrix} 2\Psi_{k-1} A_{k-1} A_{k-1}^\top \Psi_{k-1} & -2\Psi_{k-1} A_{k-1} B_k^\top \Psi_k \\ -2\Psi_k B_k A_{k-1}^\top \Psi_{k-1} & 2\Psi_k(I - A_k A_k^\top) \Psi_k \end{bmatrix}. \quad (29)$$

If A_{k-1} is zero, then it is trivial to have $H_k \succeq 0$. For nonzero A_{k-1} , we can verify that $H_k \succeq 0$ since the Schur complement to $[H_k]_{11}$ shows

$$\begin{aligned} & 2\Psi_k(I - A_k A_k^\top) \Psi_k - 2\Psi_k B_k A_{k-1}^\top \Psi_{k-1} (2\Psi_{k-1} A_{k-1} A_{k-1}^\top \Psi_{k-1})^+ 2\Psi_{k-1} A_{k-1} B_k^\top \Psi_k \\ &= 2\Psi_k(I - A_k A_k^\top - B_k B_k^\top) \Psi_k + 2\Psi_k B_k (I - A_{k-1}^+ A_{k-1}) B_k^\top \Psi_k \\ &= 2\Psi_k B_k (I - A_{k-1}^+ A_{k-1}) B_k^\top \Psi_k \succeq 0 \end{aligned}$$

where X^+ denotes the Moore–Penrose inverse of the matrix X , and it satisfies $I - X^+ X \succeq 0$.

For $k = L$ we take

$$H_L = \begin{bmatrix} 2\Psi_{L-1} A_{L-1} A_{L-1}^\top \Psi_{L-1} & -\sqrt{2\gamma} A_{L-1} B_L^\top \Psi_{L-1} \\ -\sqrt{2\gamma} \Psi_{L-1} B_L A_{L-1}^\top & \gamma I \end{bmatrix}. \quad (30)$$

Similarly, we can conclude $H_L \succeq 0$ using Schur complement

$$\gamma I - \sqrt{2\gamma} \Psi_{L-1} B_L A_{L-1}^\top (2\Psi_{L-1} A_{L-1} A_{L-1}^\top \Psi_{L-1})^+ \sqrt{2\gamma} A_{L-1} B_L^\top \Psi_{L-1} = \gamma \Psi_{L-1} B_L (I - A_{L-1}^+ A_{L-1}) B_L^\top \Psi_{L-1} \succeq 0.$$

We now show that H_k with $k = 0, \dots, L$ satisfy the chordal decomposition (27) holds since

$$\begin{aligned} [H_k]_{21} &= -2\Psi_k B_k A_{k-1}^\top \Psi_{k-1} = -\Psi_k^2 (2\Psi_k^{-1} B_k A_{k-1}^\top \Psi_{k-1}) = -\Lambda_k W_k, \\ [H_k]_{22} + [H_{k+1}]_{11} &= 2\Psi_k(I - A_k A_k^\top) \Psi_k + 2\Psi_k A_k A_k^\top \Psi_k = 2\Psi_k^2 = 2\Lambda_k. \end{aligned}$$

Finally, we conclude that $H \succeq 0$ from [37][Theorem 2.1].

Necessary. For any W_k and Λ_k satisfying (20), we will find set of free variables d_k, X_k, Y_k such that (7) holds. We take $\Psi_k = \Lambda^{\frac{1}{2}}$ which further leads to $d_k = \text{diag}(\log \Psi_k)$. By letting $A_{-1} = I, \Psi_{-1} = \sqrt{\gamma/2} I$ and $\Psi_L = \sqrt{2/\gamma} I$ we then construct A_k, B_k recursively via

$$B_k = \frac{1}{2} \Psi_k W_k \Psi_{k-1}^{-1} A_{k-1}^{-\top}, \quad A_k = \text{chol}(I - B_k B_k^\top) Q_k \quad (31)$$

where $\text{chol}(\cdot)$ denotes the Cholesky factorization, Q_k is an arbitrary orthogonal matrix such that A_k does not have eigenvalue of -1 . If A_{k-1} is non-invertible but non-zero, we replace $A_{k-1}^{-\top}$ with $(A_{k-1}^+)^{\top}$. If $A_{k-1} = 0$ (i.e. $W_k = 0$), we simply reset $A_{k-1} = I$. It is easy to verify that Ψ_k, A_k and B_k satisfy the model parameterization (7). Finally, we can construct X_k, Y_k using (36), which is well-defined as A_k does not have eigenvalue of -1 .

C.4 Proof of Theorem 3.3

The proposed layer (9) can be rewritten as a compact network (17) with $W = 0$, $Y = \sqrt{2}A^\top\Psi$ and $U = \sqrt{2}\Psi^{-1}B$, i.e.,

$$v = Uh_{\text{in}} + b, \quad z = \sigma(v), \quad h_{\text{out}} = Yz.$$

From the model parameterization (6) we have $AA^\top + BB^\top = I$, which further implies

$$2\Psi^2 - Y^\top Y - \Psi^2 U U^\top \Psi^2 = 2\Psi^2 - 2\Psi A A^\top \Psi - 2\Psi B B^\top \Psi = 2\Psi(I - A A^\top - B B^\top)\Psi = 0$$

By applying Schur complement twice to the above equation we have

$$\begin{bmatrix} I & -U^\top \Psi^2 & 0 \\ -\Psi^2 U & 2\Psi^2 & -Y^\top \\ 0 & -Y & I \end{bmatrix} \succeq 0.$$

Then, the 1-Lipschitzness of (9) is obtained by Theorem A.3.

C.5 Proof of Proposition 3.4

Sufficient. It is a direct corollary of Theorem 3.3 by taking the identity operator as the nonlinear activation.

Necessary. Here we give a constructive proof. That is, given a weight matrix W with $\|W\| \leq 1$, we will find a (generally non-unique) pair of (X, Y) such that $2A^\top B = W$ with A, B given by (6).

We first construct A, B from W . Since it is obvious for $W = 0$, we consider the case with nonzero W . First, we take a singular value decomposition (SVD) of W , i.e. $W = U_w \Sigma_w V_w^\top$ where U_w is a $q \times q$ orthogonal matrix, Σ_w is an $q \times p$ rectangular diagonal matrix with $\Sigma_{w,ii} \geq 0$ non-increasing, V_w is a $p \times p$ orthogonal matrix. Then, we consider the candidates for A and B as follows:

$$A = U \Sigma_a U_w^\top, \quad B = U \Sigma_b V_w^\top \quad (32)$$

where Σ_a is a diagonal matrix, Σ_b a rectangular diagonal matrix $U \in \mathbb{R}^{q \times q}$ an orthogonal matrix. By substituting (32) into the equalities $AA^\top + BB^\top = I_q$ and $W = 2A^\top B$ we have

$$\Sigma_a^2 + \Sigma_{b'}^2 = I_q, \quad 2\Sigma_a \Sigma_{b'} = \Sigma_{w'} \quad (33)$$

where $\Sigma_{b'}, \Sigma_{w'} \in \mathbb{R}^{q \times q}$ are obtained by either removing the extra columns of zeros on the right or adding extra rows of zeros at the bottom to Σ_b and Σ_w , respectively. The solution to (33) is

$$\Sigma_{a,ii} = \frac{1}{2} \left(\sqrt{1 + \Sigma_{w',ii}} + \sqrt{1 - \Sigma_{w',ii}} \right), \quad \Sigma_{b',ii} = \frac{1}{2} \left(\sqrt{1 + \Sigma_{w',ii}} - \sqrt{1 - \Sigma_{w',ii}} \right) \quad (34)$$

where are well-defined as $\|W\| \leq 1$. Now we can obtain Σ_b from $\Sigma_{b'}$ by removing extra rows of zeros at the bottom or adding extra columns of zeros on the right. At last, we pick up any orthogonal matrix U such that $A = U \Sigma_a U_w^\top$ does not have eigenvalue of -1 .

The next step is to find a pair of (X, Y) such that

$$A^\top = (I + Z)^{-1}(I - Z), \quad B^\top = -2Y(I + Z)^{-1}, \quad Z = X - X^\top + Y^\top Y. \quad (35)$$

One solution to the above equation is

$$Z = (I - A^\top)(I + A^\top)^{-1}, \quad Y = -\frac{1}{2}B^\top(I + Z), \quad X = \frac{1}{2}\text{tril}(Z - Z^\top) \quad (36)$$

where $\text{tril}(W)$ denotes the strictly lower triangle part of W . Note that the above solution is well-defined since A does not has eigenvalue of -1 .

C.6 Proof of Proposition 3.5

From (28) we have

$$H_0 = \begin{bmatrix} \gamma I & -W_0^\top \Psi_0^2 \\ -\Psi_0^2 W_0 & 2\Psi_0 B_0 B_0^\top \Psi_0 \end{bmatrix} \succeq 0.$$

Applying the Schur complement yields $\gamma I - 1/2W_0^\top \Psi_0 (B_0 B_0^\top)^+ \Psi_0 W_0 \succeq 0$, which implies $\|B_0^+ \Psi_0 W_0\| \leq \sqrt{2\gamma}$. From (29) we obtain

$$\begin{aligned} H_k &= \begin{bmatrix} 2\Psi_{k-1} A_{k-1} A_{k-1}^\top \Psi_{k-1} & -W_k^\top \Psi_k^2 \\ -\Psi_k^2 W_k & 2\Psi_k B_k B_k^\top \Psi_k \end{bmatrix} \succeq 0 \\ \Rightarrow \Psi_{k-1} A_{k-1} A_{k-1}^\top \Psi_{k-1} - \frac{1}{4} W_k^\top \Psi_k (B_k B_k^\top)^+ \Psi_k W_k &\succeq 0 \\ \Rightarrow I - \frac{1}{4} A_{k-1}^+ \Psi_{k-1}^{-\top} W_k^\top \Psi_k (B_k B_k^\top)^+ \Psi_k W_k \Psi_{k-1}^{-1} (A_{k-1}^\top)^+ &\succeq 0 \\ \Rightarrow \left\| \frac{1}{2} B_k^+ \Psi_k W_k \Psi_{k-1}^{-1} (A_{k-1}^\top)^+ \right\| &\leq 1. \end{aligned}$$

Similarly, from (30) we have

$$H_L = \begin{bmatrix} 2\Psi_{L-1} A_{L-1} A_{L-1}^\top \Psi_{L-1} & -W_L^\top \\ -W_L & \gamma I \end{bmatrix} \succeq 0 \Rightarrow \left\| W_L \Psi_{L-1}^{-1} (A_{L-1}^\top)^+ \right\| \leq \sqrt{2\gamma}.$$

The bound of $\mathbf{J}^c f$ is then obtained by

$$\begin{aligned} \|\mathbf{J}^c f\| &= \|W_L J_{L-1} W_{L-1} \cdots J_0 W_0\| \\ &= \left\| \frac{1}{2} W_L \Psi_{L-1}^{-1} (A_{L-1}^\top)^+ (2A_{L-1}^\top J_{L-1} B_{L-1}) \prod_{k=L-1}^1 \left(\frac{1}{2} B_k^+ \Psi_k W_k \Psi_{k-1}^{-1} (A_{k-1}^\top)^+ \right) (2A_{k-1}^\top J_{k-1} B_{k-1}) (B_0^+ \Psi_0 W_0) \right\| \\ &\leq (\sqrt{2\gamma})^2 / 2 = \gamma \end{aligned}$$

where the inequality follows as $2A_k^\top J_k B_k$ is the Clake Jacobian of a nonexpansive layer (9), i.e. $\|2A_k^\top J_k B_k\| \leq 1$.

D Experiments

Dataset. For the square wave experiment, we take 300 and 600 samples (x_i, y_i) with $x_i \sim \mathcal{U}([-2, 2])$ for training and testing, respectively. For the sine wave experiment, we take 50 and 200 points (x_i, y_i) for training and testing, where $x_i = 2i/N\pi$ with N as the size of dataset. We use batch size of 50 for those two tasks. For the CIFAR-10 dataset, we applied standard augmentation, i.e., random cropping and flipping. Inputs to all image classification models are normalized.

Model architectures for image classification benchmarks. We trained small fully-connected model on MNIST and the KWLarge network from [38] on CIFAR-10, with detailed architecture listed in Table 3. To make the different models have similar number of parameters in the same experiment, we slightly reduce the hidden layer width of sandwich model in the MNIST experiment and increases width of the first fully-connected layer of CNN and orthogonal models. We also applied the emulated 2-stride from [30] to the second and fourth convolution layers. For each experiment, we also trained a conventional MLP/CNN model with similar amount of parameters as baselines.

Training details. For all experiments, we used a piecewise triangular learning rate [39] with maximum rate in $\{0.05, 0.01, 0.005, 0.001\}$, choosing the one with the best test performance. We found that 0.01 often works

Table 3: Model architectures for image classification benchmarks.

MNIST	SANDWICH	ORTHOLOGON	MLP
FC	(190, 190, 128)	(256,256,128)	(256,256,128)
NUM. PARAMS	300,374	300,942	300,938
KWLARGE (CIFAR-10)	SANDWICH	ORTHOLOGON	CNN
CONV	(32,32,64,64)	(32,32,64,64)	(32,32,64,64)
FC	(512, 512)	(640,512)	(640,512)
NUM. PARAMS	2,982,225	2,995,373	3,020,970

well and took it as a default rate. We use Adam [40] and ReLU as our default optimizer and activation, respectively. For the image classification tasks, we used similar loss function and initialization method as [30].

Because the Cayley transform in (6) involves both linear and quadratic terms, we implemented the weight normalization method from [41]. That is, we reparameterize X, Y in $Z = X - X^\top + Y^\top Y$ by $g \frac{X}{\|X\|_F}$ and $h \frac{Y}{\|Y\|_F}$ with learnable scalars g, h . For all γ -LBDNs, we choose hidden layer to be nonexpansive (i.e., 1-Lipschitz) and put a scaling factor $\sqrt{\gamma}$ on the input and output, respectively. On the image classification tasks, we did not observe significant improvement by uniformly distributing the Lipschitz capacity, i.e., each nonexpansive hidden layer is scaled by $\gamma^{\frac{1}{L}}$. We choose Lipschitz bounds of 0.1, 0.5, 1.0 for MNIST and 1,10,100 for CIFAR-10. We search for the empirical lower Lipschitz bound $\underline{\gamma}$ of a network f_θ by a PGD-like method, i.e., updating the input x and its deviation δ_x based on the gradient of $\|f_\theta(x + \delta_x) - f_\theta(x)\|/\|\delta_x\|$. As we are interested in the global lower Lipschitz bound, we do not project x and $x + \delta_x$ into any compact region. For robustness verification, we used the L2FastGradientAttack method from the package `foolbox` [42]. All image classification experiments were performed on a Nvidia A5000.